Geophysical Research Letters

RESEARCH LETTER
10.1029/2022GL099283

The Unexpected Oceanic Peak in Energy Input to the Atmosphere and Its Consequences for Monsoon Rainfall

Nandini Ramesh[1,2] and **William R. Boos**[2,3]

[1]ARC Centre for Data Analytics for Resources and the Environment, University of Sydney, Darlington, NSW, Australia, [2]Department of Earth and Planetary Science, University of California, Berkeley, CA, USA, [3]Climate and Ecosystem Sciences Division, Lawrence Berkeley National Laboratory, Berkeley, CA, USA

Key Points:

- The maximum energy input to the atmosphere in boreal summer lies over the northern Indian Ocean
- Cloud radiative effects (CREs) strongly enhance energy input over ocean compared to land
- Surface heat capacity contrasts interact with CREs to shift monsoon rainfall

Supporting Information:

Supporting Information may be found in the online version of this article.

Correspondence to:

N. Ramesh,
nandini.ramesh@sydney.edu.au

Citation:

Ramesh, N., & Boos, W. R. (2022). The unexpected oceanic peak in energy input to the atmosphere and its consequences for monsoon rainfall. *Geophysical Research Letters*, *49*, e2022GL099283. https://doi.org/10.1029/2022GL099283

Received 26 APR 2022
Accepted 8 JUN 2022

Author Contributions:

Conceptualization: Nandini Ramesh, William R. Boos
Data curation: Nandini Ramesh
Funding acquisition: William R. Boos
Investigation: Nandini Ramesh, William R. Boos
Methodology: Nandini Ramesh, William R. Boos
Resources: William R. Boos
Validation: Nandini Ramesh, William R. Boos
Visualization: Nandini Ramesh
Writing – original draft: Nandini Ramesh, William R. Boos
Writing – review & editing: Nandini Ramesh, William R. Boos

Abstract Monsoons have historically been understood to be caused by the low thermal inertia of land, allowing more energy from summer insolation to be transferred to the overlying atmosphere than over adjacent ocean. Here, we show that during boreal summer, the global maximum net energy input (NEI) to the atmosphere unexpectedly lies over the Indian Ocean, not over land. Observed radiative fluxes suggest that cloud-radiative effects (CRE) almost double the NEI over ocean, shifting the NEI peak from land to ocean. Global climate model experiments with both land and interactive sea surface temperatures confirm that CRE create the oceanic NEI maximum. Interactions between CRE, NEI, circulation, and land-sea contrast in surface heat capacity shift precipitation from Southeast to South Asia. CRE thus alter the global partitioning of precipitation between land and ocean and the spatial structure of Earth's strongest monsoon, in ways that can be understood through the NEI.

Plain Language Summary Land's influence on the energy supplied to the atmosphere has long been recognized as a leading cause of monsoons. From early theories conceptualizing monsoons as continental-scale sea breezes responding to land-sea temperature contrasts, to modern frameworks based on air's total energy content, the energy input to the atmosphere over land has been assumed higher than that over ocean in the summer hemisphere. We show that, instead, in the Asian region, the energy input to the atmosphere is larger over ocean than land because of clouds' effects on radiation. Observations and simulations indicate that the spatial pattern of tropical rainfall is set by interactions between clouds and the land-sea contrast in surface heat capacity, mediated by atmospheric circulation.

1. Introduction

Monsoons have, for over a century, been known to be caused by land-sea contrast (Ananthakrishnan et al., 1965; Blanford, 1888). The low thermal inertia of off-equatorial land allows more energy from summer insolation to be transferred to the overlying atmosphere there than over the near-equatorial ocean; this sets up a thermally direct circulation with precipitating ascent over the continent. This precipitating circulation was traditionally seen as a continental-scale sea breeze responding to land-sea temperature contrast, but in recent decades has been better understood by including the latent heat of water vapor in measures of energy, such as the widely used moist static energy (MSE). A general understanding of controls on the structure of monsoons was obtained using a series of idealized climate models in which air's MSE is a central variable (Chou et al., 2001; Neelin, 2007; Plumb, 2007).

As an alternative to theoretical frameworks based on the energy content of air, frameworks based on energy sources, that is, the net energy input (NEI) to the atmosphere, have been explored (Biasutti et al., 2018). The NEI is the sum of surface turbulent fluxes (sensible and latent heat) and the net radiative flux into the atmospheric column; horizontal contrasts in NEI can be viewed as a forcing for tropical circulations, which are typically "energetically direct" with an ascent branch near the NEI and MSE maxima. Radiative and wind-evaporation feedbacks can render the NEI diagnostic, rather than a true exogenous forcing, but these feedbacks often exhibit substantial cancellation (Laguë et al., 2021; Peterson & Boos, 2020). The seasonal cycle of tropical precipitation maxima is strongly associated with that in NEI and, through conservation of energy, with zonal and meridional energy fluxes carried by time-mean overturning tropical atmospheric circulations (Adam et al., 2016; Boos & Korty, 2016; Donohoe et al., 2013; Kang et al., 2008).

Despite this theoretical focus on NEI as a driver of tropical circulations, few studies have examined observationally based estimates of NEI, especially with the goal of understanding how observed spatial structures influence

regional precipitation. Top-of-atmosphere (TOA) radiative fluxes have been used to show that there is positive NEI over continents in the summer hemisphere, with weaker values over ocean and strong negative NEI over continents in the winter hemisphere (Chou & Neelin, 2003); such studies argued that an energetically direct circulation results, with precipitating ascent over summer continents. A review of the dynamics of tropical convection zones and monsoons (Neelin, 2007) stated that NEI was systematically larger over land than ocean by 50–100 W m^{-2}, with that contrast driving planetary-scale monsoon flow. Here, we highlight a surprising deviation from this view of land-ocean contrast: an oceanic maximum in NEI that we show strongly influences the spatial structure of precipitation in Asia. We build on prior studies of cloud radiative effects (CRE) in monsoons (J. Li et al., 2017; Rajeevan & Srinivasan, 2000; Sharma, 1998) to show that CRE play a key role in setting this spatial pattern of NEI (Section 4). Using a general circulation model (GCM) that, unlike in prior studies of the influence of CRE on precipitation (Byrne & Zanna, 2020; Voigt & Albern, 2019), accounts for the differing thermal inertia between ocean and land, we show that differences in the response of the land and sea surface to CRE establish this oceanic NEI maximum and set the structure of precipitation (Section 5).

2. Materials and Methods

This study uses atmospheric reanalyses, observations, and a global climate model. All data used here are publicly available. Figures 1 and 2 use the European Center for Medium-Range Weather Forecasts (ECMWF) Reanalysis Version 5 (ERA5; Hersbach et al., 2020; 1979–2018) so as to display an internally consistent estimate of NEI and its components. Findings reported here were verified against other reanalyses and observational products, listed below. Conclusions were based only on features for which all listed data sets displayed qualitative agreement.

2.1. Reanalysis Products

In addition to ERA5, we use surface turbulent and radiative fluxes and TOA radiative fluxes from these reanalyses in Figure 1c:

1. The National Center for Environmental Prediction Climate Forecast System Reanalysis, Version 2 **(CFSR)** (Saha et al., 2014; 1979–2016).
2. The ECMWF Interim Reanalysis **(ERA-I)** (Dee et al., 2011; 1979–2015).
3. The Japanese Meteorological Agency 55 yr Reanalysis **(JRA)** (Kobayashi et al., 2015; 1979–2008).
4. The National Aeronautics and Space Administration (NASA) Modern-Era Retrospective Analysis for Research and Applications, version 2 **(MERRA2)** (Gelaro et al., 2017; 1980–2015).
5. The National Center for Environmental Prediction-Department of Energy Reanalysis II **(NCEP)** (Kanamitsu et al., 2002; 1948–2018).

2.2. Observational Products

We also use the following observational estimates of ocean surface fluxes, surface and TOA radiative fluxes, cloud fraction, and precipitation:

2.2.1. Air-Sea Turbulent Fluxes

1. The National Oceanography Center Surface Flux and Meteorological Data Set **(NOCS)** (Berry & Kent, 2009; 2000–2018)
2. The Woods Hole Oceanographic Institution Objectively Analyzed Air-Sea Flux Project, version 3 **(OAFlux)** (Yu & Weller, 2007; 1958–2018)
3. The National Oceanic and Atmospheric Administration (NOAA) Climate Data Record of Ocean Heat Fluxes, version 2 **(SeaFlux)** (Clayson et al., 2016; 2000–2020)

2.2.2. Radiative Fluxes

Clouds and the Earth's Radiant Energy System Energy Balanced and Filled TOA edition-4.0 data product **(CERES)** (Loeb et al., 2018). In figures where this is combined with other data sets, the overlapping years of 2000–2018 are used.

2.2.3. Cloud Fraction

The Cloud-Aerosol Lidar and Infrared Pathfinder Satellite Observations (CALIPSO) GCM-Oriented Cloud CALIPSO Product **(CALIPSO-GOCCP)** (Chepfer et al., 2010; 2001–2018). In Figure S2 in Supporting Information S1, we use CALIPSO-GOCCP's definition of high clouds, that is, clouds above 6.5 km altitude, to calculate high cloud fraction. High cloud fraction is computed as the maximum cloud area fraction over all layers higher than this threshold.

2.2.4. Precipitation

The Global Precipitation Climatology Project **(GPCP)** version 2.3 (Adler et al., 2018). A climatology was calculated using monthly means from 1979 to 2020.

2.3. Estimation of NEI

We estimate the NEI as the sum of upward surface turbulent fluxes, upward surface radiative fluxes, and downward TOA radiative fluxes. All terms needed to calculate this quantity are included in the reanalyses.

For observational estimates, we use TOA and surface radiative fluxes from CERES with turbulent surface fluxes over ocean from each of the observational products listed. It is difficult to obtain estimates of the global distribution of surface turbulent fluxes over land; however, due to the low heat capacity of land, the net land surface energy flux is near zero on seasonal timescales and therefore the NEI is nearly equal to the TOA flux over land (Neelin, 2007). In some regions, a small amount of energy (generally not exceeding 20 W m^{-2}) is consumed at the surface through processes such as seasonal snowmelt; we account for this by computing the difference between NEI and TOA flux over land from ERA5 and applying this as a correction to arrive at the NEI over land in Figure 1c.

2.4. Global Climate Model Experiments

We use the Community Earth System Model (CESM) version 2.0, with the scientifically validated "ETEST" component set. This consists of a global atmosphere model at a resolution of 2.5° × 1.875° with 32 vertical levels, coupled to a slab ocean 30 m deep, using a climatological q-flux (i.e., a spatially varying heat flux in the ocean representing the effects of ocean heat transport and processes such as ice melt/freezing) derived from a coupled control run of the model. In this component set, the Community Land Model (CLM5.0) is used with satellite phenology, and greenhouse gas concentrations are held at pre-industrial (year 1850) levels. A 5 yr spinup was used before the experiments were performed.

Because we focus on the impacts of cloud-radiative effects during boreal summer, we initiate all experiments from 1 May of the sixth year of a control run. This prevents model drift due to the altered conditions in the experiments from affecting the season of interest. The "noTropicCloud" experiment consists of an ensemble of five simulations in which radiative effects of clouds within the latitudes 35°S–35°N were set to zero, that is, clouds within the tropical belt were transparent to both shortwave and longwave radiation. This is similar to the method used in the Clouds On-Off Klimate Intercomparison Experiment (COOKIE; Stevens et al., 2012), except using prognostic instead of prescribed SST. The latitude of 35° was chosen as it corresponds to the latitude where the annual-mean, zonal-mean TOA fluxes change sign. Each of the five simulations was initiated with a different small perturbation.

The control experiment consists of a similarly designed ensemble, with CRE active. Results presented are averaged over these ensembles. In figures where differences between the control and noTropicCloud are shown, only areas where differences were significant at the 95% level based on a two-tailed *t* test are shaded.

3. The Observed Distribution of NEI

During local summer in each hemisphere, NEI is typically largest over land (Figures 1a and 1b), acting as an energy source for the circulation. This pattern is consistent with the view that monsoon circulations are driven by a continental energy source maximum (Neelin, 2007). For South Asia, however, the atmosphere gains substantially more energy over the Bay of Bengal than over adjacent land, which is, according to several data sets, the global maximum of NEI in boreal summer. Despite wide variation in the estimated NEI across reanalyses and observational products (Figure 1c), all display an NEI peak over the Northern Indian Ocean.

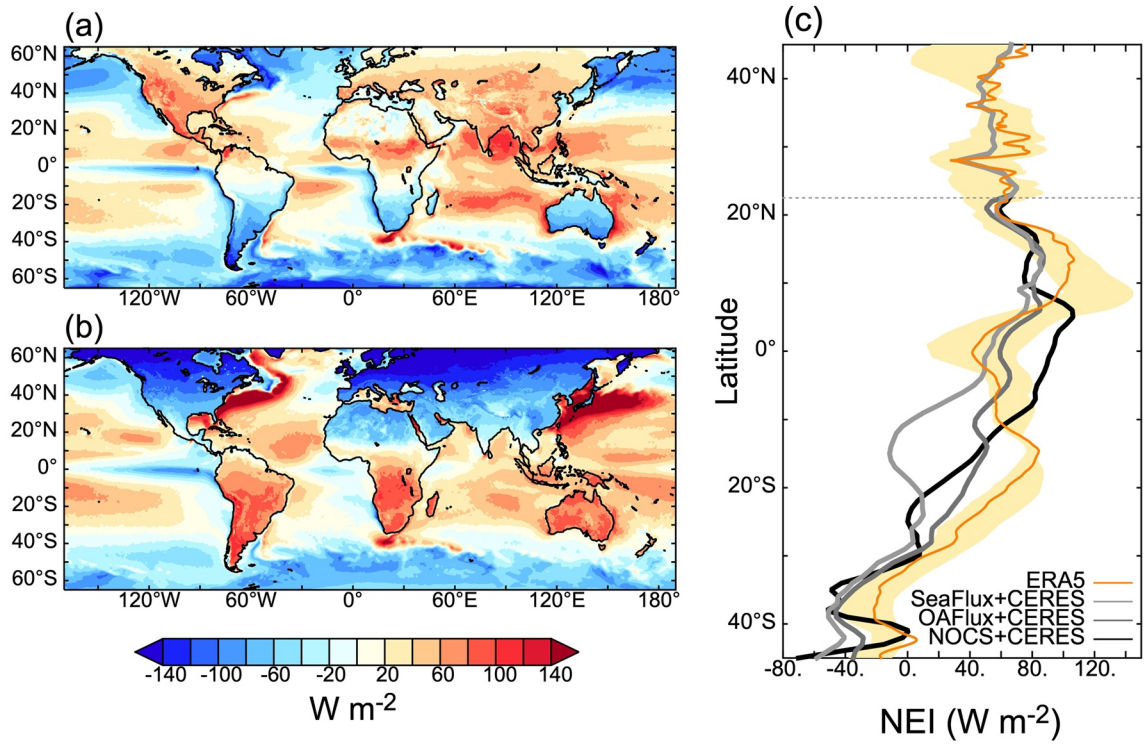

Figure 1. The oceanic nature of the energy input maximum during boreal summer: The climatological net energy input (NEI; W/m^2) to the atmospheric column in (a) boreal summer (June–August) and (b) austral summer (December–February) from ERA5. (c) NEI into the atmosphere from three observational estimates (thick gray lines) and ERA5 (orange line) averaged over the longitudes of the Bay of Bengal (90°E–95°E) in boreal summer. The filled area indicates the range of the same quantity from five other reanalysis products (listed in Section 2.1). The dotted line indicates the latitude of the northern edge of the Bay of Bengal.

We decompose the NEI into surface and TOA components, showing that the net surface energy flux (including radiation) is near zero or negative over the Bay of Bengal and Arabian Sea during boreal summer, despite the large surface turbulent heat fluxes into the atmosphere there (Figure 2a, Figure S1 in Supporting Information S1). Over the Northern Indian Ocean, TOA fluxes contribute most of the positive NEI (Figure 2b), suggesting a role played by processes that influence TOA radiation, such as clouds. The shortwave and longwave components of the CRE (Figure 2c) confirm this: while the shortwave effect of clouds reflects energy into space and is therefore negative over the region experiencing monsoon rainfall, the longwave effect, which retains energy in the atmospheric column, is largest over the Bay of Bengal NEI maximum. This reduction in energy loss to space coincides with an area covered by high cloud tops (Figure S2 in Supporting Information S1); the frequent occurrence of organized mesoscale convective systems in this region likely contributes to this large high-cloud fraction (P. J. Chen et al., 2021; Hamada et al., 2014; Luo et al., 2017; Yuan & Houze, 2010). The resulting net CRE (Figure 2d) thus makes a large positive contribution to the NEI over the northern Indian Ocean.

4. The Prognostic Influence of CREs

While observed radiative fluxes can be used to estimate the net influence of clouds on radiation given the observed atmospheric state (e.g., Figure 2d), it is possible that large changes in wind, temperature, humidity, and cloud properties would occur in the absence of CRE. This motivates our use of the climate model described in Section 2 to determine, prognostically, the influence of CRE on both the NEI and the large-scale circulation.

The control run captures key features of the NEI distribution, including the energy sources over ocean in the Southern Hemisphere and Northern Hemisphere continents, and the maximum over the northern Indian Ocean during boreal summer (Figure 3a). There is some bias relative to ERA5, but this is of comparable magnitude to the observational uncertainty in NEI (e.g., Figure 1c). The CRE contribution to NEI (Figure 3b), calculated as

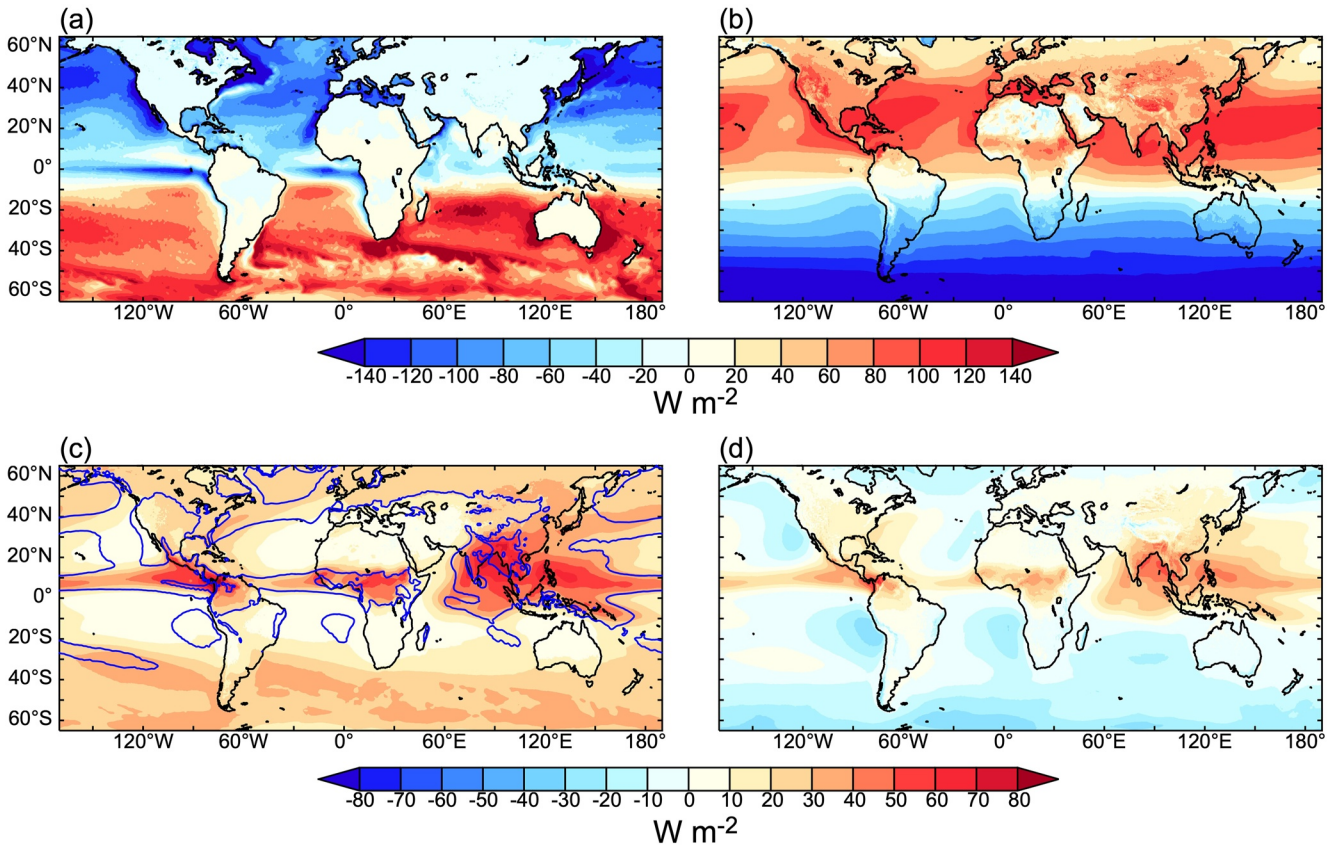

Figure 2. Components of the observed energy input: The contributions of fluxes at (a) the surface and (b) the top of the atmosphere to the climatological net energy input (NEI). Panel (c) shows the contributions of the longwave (colors) and shortwave (contours; intervals of −50 Wm^{-2}) components of cloud radiative effect (CRE) respectively. The total estimated contribution of CRE is shown in (d). Quantities are positive if they contribute to the energy content of the atmospheric column.

the difference between clear-sky and all-sky radiative effects, in the control run is similar to that in observations (Figure 2d).

Examining the difference between the control run and the run with CRE eliminated in the tropics (the noTropicCloud experiment), confirms that clouds enhance NEI over the entire Northern Indian Ocean (Figure 3c). However, tropical CRE also reduces NEI over several land areas, particularly Southeast Asia. Overall, the response to removing clouds in the model experiment differs greatly from the CRE inferred simply as the difference between all-sky and clear-sky radiative effects (Figure 3b), indicating that CRE induces feedbacks on surface turbulent fluxes and radiation.

The absence of CRE substantially alters boreal summer precipitation (Figure 3d). Notably, including CRE reduces rainfall over tropical land relative to that over ocean. The fraction of total summer rainfall within the latitude range of eliminated CRE (35°S–35°N) that occurs over land increases from 0.2 in the control to 0.25 in the noTropicCloud experiment (a relative increase of 26% [±4%, one standard deviation]); in the deep tropics (20°S–20°N), this re-partitioning of rainfall over land versus ocean is even more pronounced, with a relative increase of 31% (±7%).

The spatial pattern of changes to rainfall is dominated by shifts in precipitation maxima. Over the Atlantic and East Pacific, the oceanic ITCZ is displaced to the north when CRE are included. This is consistent with previous aquaplanet studies (Voigt et al., 2014) that concluded that CRE shift the ITCZ poleward by producing interhemispheric NEI asymmetries. Over the Indo-Pacific, however, the spatial pattern of changes in precipitation is more complex, displaying a striking southwestward shift of rainfall from East Asia to South Asia when CRE is added.

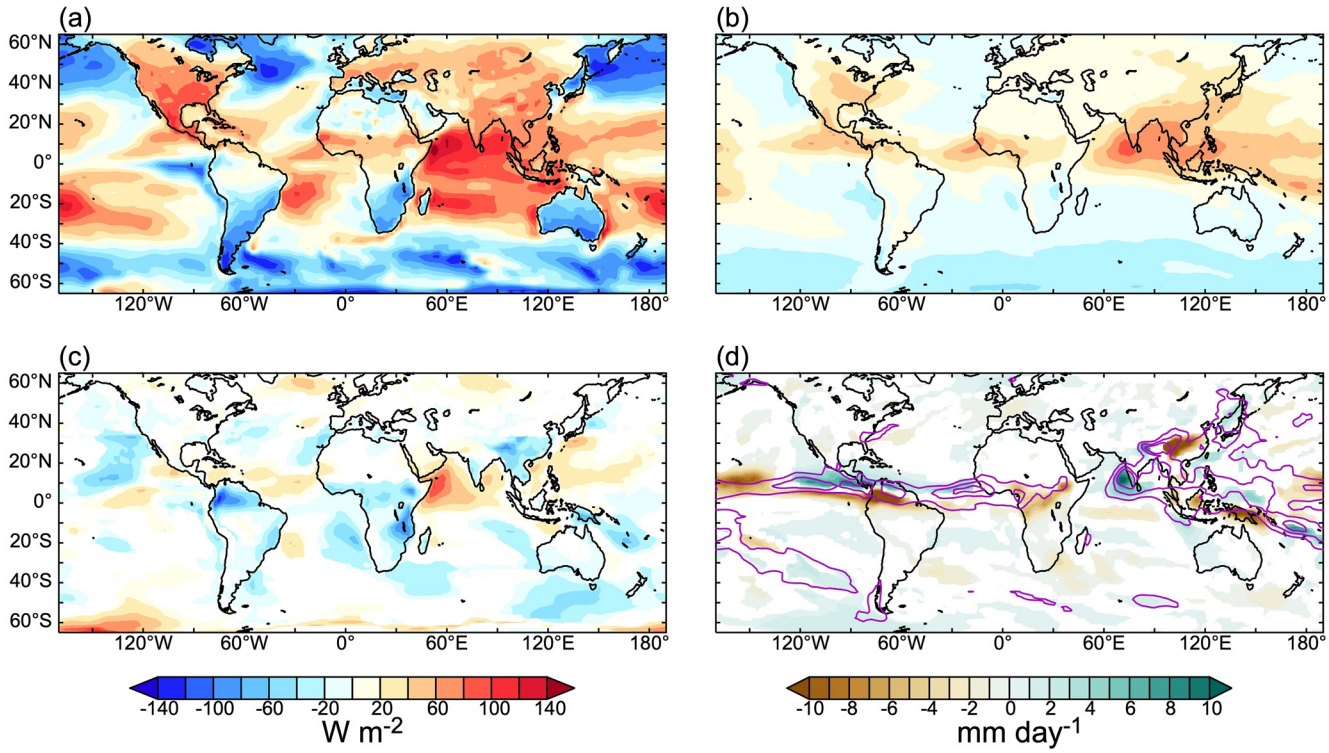

Figure 3. Perturbing cloud-radiative effects in a global model: the June–August mean (a) net energy input (NEI), and (b) cloud-radiative effect (CRE) contribution to NEI from the control ensemble, calculated as the difference between all-sky and clear-sky radiative effects. The bottom row shows the June–August mean contribution of CRE inferred prognostically (control minus noTropicCloud) (c) to NEI and (d) to precipitation. Contours in (d) indicate the June–August mean precipitation in the control ensemble at 5 mm/day increments.

5. The Influence of CREs on Atmospheric Circulation

The cause of this mostly zonal shift over Asia can be understood using dynamic or energetic perspectives. We first describe how CRE alter the distributions of precipitation, surface enthalpy fluxes, and MSE advection, then use an energetic framework to show how the influence of clouds on NEI is quantitatively consistent with the model-simulated precipitation shift.

We treat the noTropicCloud experiment as a basic state on which CRE can be applied. In that state, boreal summer precipitation peaks over southeastern Asia (Figure 4a, gray contours), consistent with idealized model simulations that show monsoon precipitation concentrates over the eastern part of rectangular tropical continents due to the Rossby gyres that comprise three-dimensional monsoon circulations (Chou et al., 2001; Privé & Plumb, 2007; S. P. Xie et al., 1999). In those studies, much of this concentration of rainfall over the eastern part of the continent is due to advection of dry air by the lower-tropospheric Rossby gyre. We see evidence for that in the noTropicCloud run: the strong zonal MSE gradient over South Asia (Figure 4a) is spanned by low-level eastward winds that feed into the region of peak precipitating ascent (Figure 4b), as expected for the linear Rossby gyre component of a monsoon (Gill, 1980; Hoskins & Rodwell, 1995). The resulting advection of MSE, vertically integrated over the atmosphere, provides a negative energy tendency over much of South and Southwest Asia exceeding 150 W m^{-2} (Figure 4b). Horizontal advection by the Rossby gyre thus greatly compensates the radiative forcing for precipitation over South Asia in the absence of CRE.

With tropical CRE turned on, the shortwave effects of clouds over southeastern Asia reduce surface enthalpy fluxes there by about 100 W m^{-2} (Figure 4c). Although the longwave effects warm the atmosphere by 30–50 W m^{-2}, opposing the shortwave contribution to the NEI, the net CRE is negative, weakening the thermally forced Rossby gyre. CRE also convectively stabilize the troposphere, as evidenced by the upper-tropospheric warming and lower-tropospheric cooling seen in the response to tropical CRE (Figure S3 in Supporting Information S1). This convective stabilization over land leads to a reduction in precipitating ascent over Southeast Asia (Figure 4e),

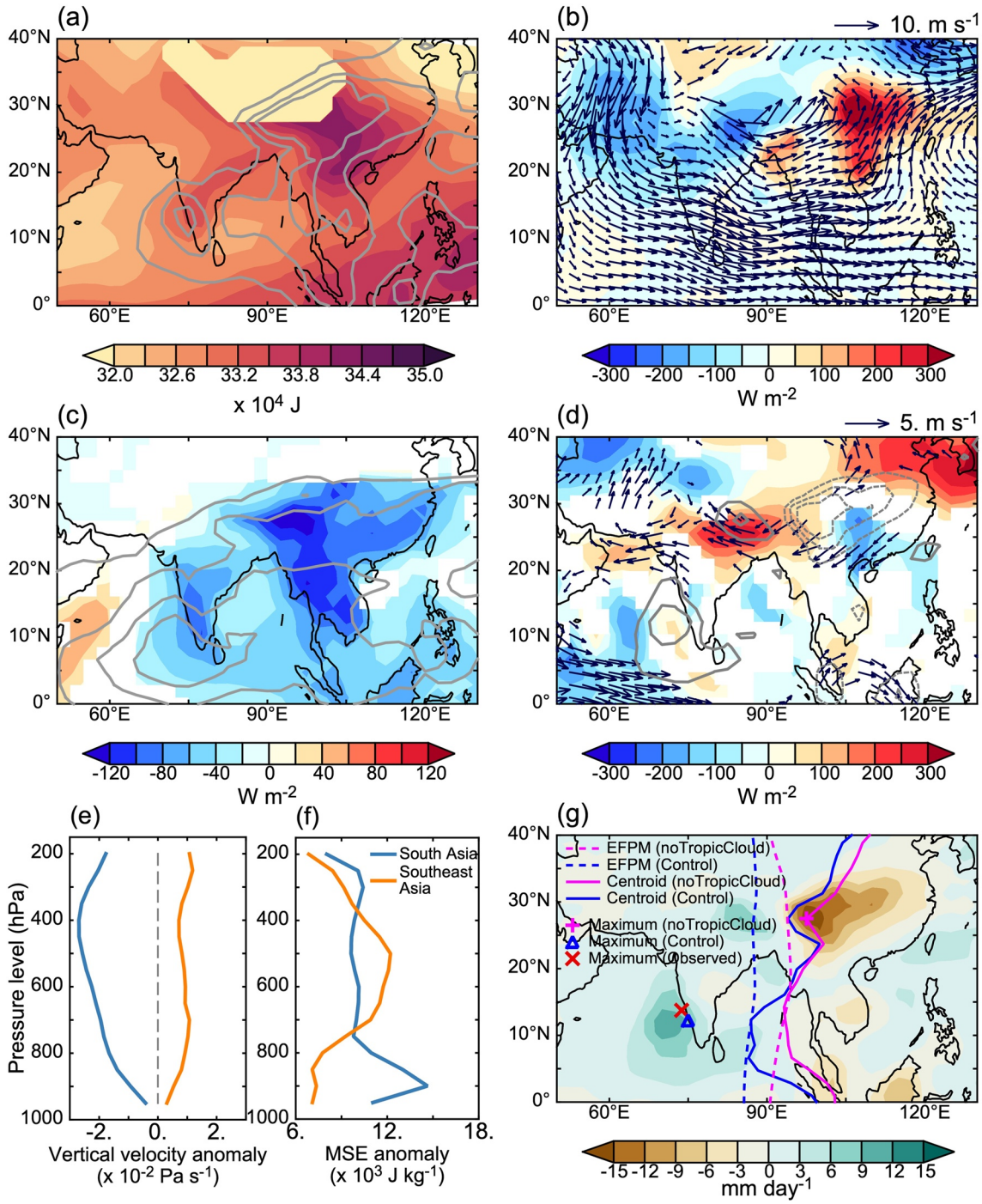

Figure 4. Cloud-radiative effects (CRE) induce a westward shift and weakening of the precipitating Rossby gyre over Asia: (a) precipitation (gray contours, interval 5 mm day^{-1}) and moist static energy (MSE) at 700 hPa (shading) in the noTropicCloud experiment. (b) Vertically integrated MSE advection in the absence of CRE (shading) with wind velocity (arrows) at 700 hPa. (c) The anomaly (control minus NoTropicCloud) in surface turbulent fluxes (shading, W m^{-2}) and column-integrated radiative flux convergence (gray contours, interval 20 W m^{-2}, negative contours dashed and zero contour omitted). (d) Anomaly (control minus NoTropicCloud) in the quantities shown in (b) and precipitation (gray contours, interval 5 mm day^{-1}, negative contours dashed and zero contour omitted). (e and f) show the anomaly (control minus noTropicCloud) in vertical velocity and MSE, respectively, averaged over South (70°E−90°E, 10°N−30°N) and Southeast (90°E−110°E, 10°N−30°N) Asia. (g) Anomaly (control minus noTropicCloud) in precipitation (shading) with the energy flux prime meridian (EFPM; dashed lines) and precipitation centroid (solid lines). Symbols indicate the location of maximum seasonal-mean precipitation.

a weakening of the low-level eastward inflow to that region, and a reduction in the negative MSE advection over northern India accomplished by that inflow (Figure 4d). This reduction in negative MSE advection peaks around 200 W m^{-2}, and is accompanied by enhanced low-level MSE over South Asia and increased precipitation there (Figure 4f); note the MSE increase over Southeast Asia peaks in the mid-troposphere, consistent with its modification by free-tropospheric CRE rather than low-level moisture advection. In summary, CRE convectively stabilizes the continental precipitation maximum and weakens the associated Rossby gyre, reducing the dry air advection that would otherwise suppress precipitating ascent over South Asia (Figure 4e).

One can alternatively view this process in terms of the influence of CRE on NEI over land, which is negative because the shortwave part of CRE exceeds the longwave part there. A negative NEI anomaly is thus induced over Southeast Asia by CRE, and this must be balanced by an anomalous flux of energy into the region, which in the tropics is typically accomplished by time-mean overturning circulations (Boos & Korty, 2016; Kang et al., 2008). Figure 4g shows the energy flux prime meridian (EFPM) in the control and noTropicCloud experiment, with the EFPM being the zero line of the divergent eastward energy flux (vertically integrated over the atmosphere); the EFPM is expected to move together with zonal shifts in zonal overturning circulations (Boos & Korty, 2016), similar to the way the energy flux equator moves with meridional shifts in meridional overturning circulations (Kang et al., 2008). The inclusion of CRE, by altering the spatial pattern of NEI, shifts the EFPM westward by 5.8°, closely matching the location of the EFPM in reanalyses over the Bay of Bengal (Boos & Korty, 2016). A corresponding westward shift in precipitation occurs, with the precipitation centroid moving 4.3° westward in the meridional mean over the region shown. This constitutes good agreement, as shifts in the zero lines of divergent energy flux are typically highly correlated with but larger than the shifts in precipitation maxima (Kang et al., 2008; Shekhar & Boos, 2016). Including CRE also shifts the precipitation maximum from continental Southeast Asia to its observed location over ocean (Figure 4g).

6. Discussion

Our analysis of the observed NEI distribution revealed that in boreal summer, the global maximum NEI is positioned over the northern Indian Ocean rather than over land, challenging the conventional view that large-scale tropical circulations in solstice seasons are associated with continental NEI maxima. When the NEI was decomposed, CRE were found to be the primary contributor to this maximum. This is distinct from other observed NEI maxima over oceans, where turbulent surface fluxes dominate (e.g., the western boundary currents and trade wind regions in the winter hemisphere; Figures 1a and 1b).

Prior studies have examined the distribution of CRE in monsoons, showing, for example, that the observed net CRE in the Asian monsoon is negative (Rajeevan & Srinivasan, 2000), and that net CRE over Asia is more negative for higher-altitude cloud tops (Saud et al., 2016). In simulations with realistic boundary conditions, CRE have been shown to amplify natural modes of Asian monsoon variability (Lu et al., 2021). Previous aquaplanet studies identified meridional shifts of precipitation maxima in response to CRE (Byrne & Zanna, 2020; Harrop & Hartmann, 2016; Popp & Silvers, 2017; Randall et al., 1989; Voigt et al., 2014); in contrast, we found that with realistic continents, the primary response to CRE over Asia is instead a zonal shift. This zonal shift is produced by the contrasting effects of CRE over land and ocean combined with the three-dimensional large-scale tropical circulation. Over land, low surface heat capacity allows the shortwave effect of clouds to cool the surface and convectively stabilize the atmosphere; over ocean, shortwave CRE has a weaker effect due to the ocean's high heat capacity. This means that over ocean, longwave CRE is the dominant contributor to the NEI, warming the atmosphere (Randall et al., 1989) even though shortwave and longwave CRE approximately cancel at TOA (Tian & Ramanathan, 2002).

The asymmetry in CRE between ocean and land is reflected in the large increase in the proportion of rainfall occurring over land when CRE is eliminated (a relative increase of 26%) and the inland shift of the location of maximum precipitation (Figure 4g). When the NEI and convective instability are reduced in the region of the precipitation maximum, the Rossby gyre circulation weakens, allowing precipitation to shift westward. This reduction in convective activity over land is consistent with theoretical models showing that CRE provides a negative feedback on the response to forcings over land (Zeng & Neelin, 1999), in contrast with the positive feedback on circulations that CRE can provide over ocean (Su & Neelin, 2002). The dry and wet biases in CESM and many other climate models over continental South (Sperber et al., 2013; S. Xie et al., 2012) and Southeast Asia

(W. T. Chen et al., 2019; Ma et al., 2014), respectively, suggest that the true magnitude of this response may be larger than that seen in our experiments.

Our findings prompt a rethinking of the role of land-sea contrast in setting the distribution of tropical NEI: in the largest monsoon system, the NEI maximum lies over ocean instead of land. Our findings also highlight the importance of differences between the land and ocean response to CRE. While CRE have long been recognized as a crucial process in atmospheric circulation (Y. Li et al., 2015; Randall et al., 1989; Sherwood et al., 1994; Slingo & Slingo, 1988; Sohn & Smith, 1992; Tian & Ramanathan, 2002) and a key determinant of its response to increasing greenhouse gas concentrations (Ceppi et al., 2017; Ceppi & Hartmann, 2016; Hansen et al., 1984; Voigt & Albern, 2019; Voigt & Shaw, 2015), they have frequently been studied in aquaplanets (Byrne & Zanna, 2020; Ceppi & Hartmann, 2016; Harrop & Hartmann, 2016; Randall et al., 1989; Voigt et al., 2014; Voigt & Shaw, 2015) or settings where the ocean's heat capacity is unaccounted for (Hansen et al., 1984; Y. Li et al., 2015; Sherwood et al., 1994; Slingo & Slingo, 1988). The results of this study suggest that the way forward in understanding the impacts of CRE on atmospheric circulation and patterns of precipitation must necessarily include the effects of spatial contrasts in the heat capacity of the underlying surface.

Data Availability Statement

All observational and reanalysis data used in this study, as described in Section 2, are publicly available from the sources listed below:

- ERA5 (Hersbach et al., 2020): https://confluence.ecmwf.int/display/CKB/How+to+download+ERA5
- CFSR (Saha et al., 2014): https://www.ncei.noaa.gov/access/metadata/landing-page/bin/iso?id=gov.noaa.ncdc:C00765
- JRA (Kobayashi et al., 2015): https://jra.kishou.go.jp/JRA-55/index_en.html
- MERRA2 (Gelaro et al., 2017): https://disc.gsfc.nasa.gov/datasets?sort=-timeRes&project=MERRA-2
- NCEP (Kanamitsu et al., 2002): https://psl.noaa.gov/data/gridded/data.ncep.reanalysis2.html
- NOCS (Berry & Kent, 2009): https://noc.ac.uk/science/sustained-observations/noc-surface-flux-dataset
- OAFlux (Yu & Weller, 2007): http://apdrc.soest.hawaii.edu/datadoc/whoi_oafluxmon.php
- SeaFlux (Clayson et al., 2016): https://seaflux.org/data-2/data
- CERES (Loeb et al., 2018): https://ceres.larc.nasa.gov/data/
- CALIPSO-GOCCP (Chepfer et al., 2010): https://climserv.ipsl.polytechnique.fr/cfmip-obs/
- GPCP (Adler et al., 2018): http://eagle1.umd.edu/GPCP_ICDR/

The output of the described climate model experiments, along with instructions to reproduce the experiments, are available in a Zenodo repository (https://doi.org/10.5281/zenodo.5704060).

Acknowledgments
N.R. was partially supported by the Australian Research Council (Data Analytics for Resources and Environments, Grant IC190100031) during the completion of this work. This material is based on work supported by the U.S. Department of Energy (DOE), Office of Science, Office of Biological and Environmental Research, Climate and Environmental Sciences Division, Regional and Global Model Analysis Program, under Award DE-SC0019367. It used resources of the National Energy Research Scientific Computing Center (NERSC), which is a DOE Office of Science User Facility. Open access publishing facilitated by The University of Sydney, as part of the Wiley - The University of Sydney agreement via the Council of Australian University Librarians.

References

Adam, O., Bischoff, T., & Schneider, T. (2016). Seasonal and interannual variations of the energy flux equator and ITCZ. Part I: Zonally averaged ITCZ position. *Journal of Climate*, *29*(9), 3219–3230. https://doi.org/10.1175/jcli-d-15-0512.1

Adler, R. F., Sapiano, M. R., Huffman, G. J., Wang, J.-J., Gu, G., Bolvin, D., et al. (2018). The Global Precipitation Climatology Project (GPCP) monthly analysis (new version 2.3) and a review of 2017 global precipitation. *Atmosphere*, *9*(4), 138. https://doi.org/10.3390/atmos9040138

Ananthakrishnan, R., Ramakrishnan, A., Selvam, M. M., & Rajagopalachari, P. (1965). Seasonal variations in the zonal and meridional circulation over India. *Current Science*, *34*(9), 272–277.

Berry, D. I., & Kent, E. C. (2009). A new air-sea interaction gridded data set from ICOADS with uncertainty estimates. *Bulletin of the American Meteorological Society*, *90*(5), 645–656. https://doi.org/10.1175/2008bams2639.1

Biasutti, M., Voigt, A., Boos, W. R., Braconnot, P., Hargreaves, J. C., Harrison, S. P., et al. (2018). Global energetics and local physics as drivers of past, present, and future monsoons. *Nature Geoscience*, *11*(6), 392–400. https://doi.org/10.1038/s41561-018-0137-1

Blanford, H. F. (1888). The rainfall of India. *Quarterly Journal of the Royal Meteorological Society*, *14*, 163–168.

Boos, W. R., & Korty, R. L. (2016). Regional energy budget control of the intertropical convergence zone and application to mid-holocene rainfall. *Nature Geoscience*, *9*(12), 892–897. https://doi.org/10.1038/ngeo2833

Byrne, M. P., & Zanna, L. (2020). Radiative effects of clouds and water vapor on an axisymmetric monsoon. *Journal of Climate*, *33*(20), 8789–8811. https://doi.org/10.1175/jcli-d-19-0974.1

Ceppi, P., Brient, F., Zelinka, M. D., & Hartmann, D. L. (2017). Cloud feedback mechanisms and their representation in global climate models. *Wiley Interdisciplinary Reviews: Climate Change*, *8*(4), e465. https://doi.org/10.1002/wcc.465

Ceppi, P., & Hartmann, D. L. (2016). Clouds and the atmospheric circulation response to warming. *Journal of Climate*, *29*(2), 783–799.

Chen, P.-J., Chen, W.-T., Wu, C.-M., & Yo, T.-S. (2021). Convective cloud regimes from a classification of object-based CloudSat observations over Asian-Australian monsoon areas. *Geophysical Research Letters*, *48*(10), e2021GL092733. https://doi.org/10.1029/2021gl092733

Chen, W.-T., Wu, C.-M., & Ma, H.-Y. (2019). Evaluating the bias of South China Sea summer monsoon precipitation associated with fast physical processes using a climate model hindcast approach. *Journal of Climate*, *32*(14), 4491–4507. https://doi.org/10.1175/jcli-d-18-0660.1

Chepfer, H., Bony, S., Winker, D., Cesana, G., Dufresne, J., Minnis, P., et al. (2010). The GCM-oriented CALIPSO cloud product (CALIPSO-GOCCP). *Journal of Geophysical Research: Atmospheres*, *115*(D4). https://doi.org/10.1029/2009jd012251

Chou, C., & Neelin, J. D. (2003). Mechanisms limiting the northward extent of the northern summer monsoons over North America, Asia, and Africa. *Journal of Climate*, *16*(3), 406–425. https://doi.org/10.1175/1520-0442(2003)016<0406:mltneo>2.0.co;2

Chou, C., Neelin, J. D., & Su, H. (2001). Ocean-atmosphere-land feedbacks in an idealized monsoon. *Quarterly Journal of the Royal Meteorological Society*, *127*(576), 1869–1891. https://doi.org/10.1002/qj.49712757602

Clayson, C. A., Brown, J., & NOAA CDR Program. (2016). *NOAA Climate Data Record (CDR) of ocean heat fluxes, version 2*. NOAA National Center for Environmental Information. Retrieved from https://data.nodc.noaa.gov/cgi-bin/iso?id=gov.noaa.ncdc:C00973 (Ocean Heat Fluxes; SeaFlux OSB CDR: Heat Fluxes).

Dee, D. P., Uppala, S. M., Simmons, A., Berrisford, P., Poli, P., Kobayashi, S., et al. (2011). The era-interim reanalysis: Configuration and performance of the data assimilation system. *Quarterly Journal of the Royal Meteorological Society*, *137*(656), 553–597. https://doi.org/10.1002/qj.828

Donohoe, A., Marshall, J., Ferreira, D., & Mcgee, D. (2013). The relationship between ITCZ location and cross-equatorial atmospheric heat transport: From the seasonal cycle to the last glacial maximum. *Journal of Climate*, *26*(11), 3597–3618. https://doi.org/10.1175/jcli-d-12-00467.1

Gelaro, R., McCarty, W., Suárez, M. J., Todling, R., Molod, A., Takacs, L., et al. (2017). The modern-era retrospective analysis for research and applications, version 2 (MERRA-2). *Journal of Climate*, *30*(14), 5419–5454. https://doi.org/10.1175/jcli-d-16-0758.1

Gill, A. E. (1980). Some simple solutions for heat-induced tropical circulation. *Quarterly Journal of the Royal Meteorological Society*, *106*(449), 447–462. https://doi.org/10.1002/qj.49710644905

Hamada, A., Murayama, Y., & Takayabu, Y. N. (2014). Regional characteristics of extreme rainfall extracted from TRMM PR measurements. *Journal of Climate*, *27*(21), 8151–8169. https://doi.org/10.1175/jcli-d-14-00107.1

Hansen, J., Lacis, A., Rind, D., Russell, G., Stone, P., Fung, I., et al. (1984). Climate sensitivity: Analysis of feedback mechanisms. *Geophysical Monograph Series*, *1*, 1–3. https://doi.org/10.1029/gm029p0130

Harrop, B. E., & Hartmann, D. L. (2016). The role of cloud radiative heating in determining the location of the ITCZ in aquaplanet simulations. *Journal of Climate*, *29*(8), 2741–2763. https://doi.org/10.1175/jcli-d-15-0521.1

Hersbach, H., Bell, B., Berrisford, P., Hirahara, S., Horányi, A., Muñoz-Sabater, J., et al. (2020). The ERA5 global reanalysis. *Quarterly Journal of the Royal Meteorological Society*, *146*(730), 1999–2049. https://doi.org/10.1002/qj.3803

Hoskins, B. J., & Rodwell, M. J. (1995). A model of the Asian summer monsoon. Part I: The global scale. *Journal of the Atmospheric Sciences*, *52*(9), 1329–1340. https://doi.org/10.1175/1520-0469(1995)052<1329:amotas>2.0.co;2

Kanamitsu, M., Ebisuzaki, W., Woollen, J., Yang, S.-K., Hnilo, J., Fiorino, M., & Potter, G. (2002). NCEP-DOE AMIP-II reanalysis (R-2). *Bulletin of the American Meteorological Society*, *83*(11), 1631–1644. https://doi.org/10.1175/bams-83-11-1631(2002)083<1631:nar>2.3.co;2

Kang, S. M., Held, I. M., Frierson, D. M., & Zhao, M. (2008). The response of the ITCZ to extratropical thermal forcing: Idealized slab-ocean experiments with a GCM. *Journal of Climate*, *21*(14), 3521–3532. https://doi.org/10.1175/2007jcli2146.1

Kobayashi, S., Ota, Y., Harada, Y., Ebita, A., Moriya, M., Onoda, H., et al. (2015). The JRA-55 reanalysis: General specifications and basic characteristics. *Journal of the Meteorological Society of Japan. Series II*, *93*(1), 5–48. https://doi.org/10.2151/jmsj.2015-001

Laguë, M. M., Swann, A. L., & Boos, W. R. (2021). Radiative feedbacks on land surface change and associated tropical precipitation shifts. *Journal of Climate*, *34*, 6651–6672. https://doi.org/10.1175/JCLI-D-20-0883.1

Li, J., Wang, W. C., Dong, X., & Mao, J. (2017). Cloud-radiation-precipitation associations over the Asian monsoon region: An observational analysis. *Climate Dynamics*, *49*, 3237–3255. https://doi.org/10.1007/S00382-016-3509-5/FIGURES/13

Li, Y., Thompson, D. W., & Bony, S. (2015). The influence of atmospheric cloud radiative effects on the large-scale atmospheric circulation. *Journal of Climate*, *28*(18), 7263–7278. https://doi.org/10.1175/jcli-d-14-00825.1

Loeb, N. G., Doelling, D. R., Wang, H., Su, W., Nguyen, C., Corbett, J. G., et al. (2018). Clouds and the Earth's Radiant Energy System (CERES) Energy Balanced and Filled (EBAF) Top-of-Atmosphere (TOA) edition-4.0 data product. *Journal of Climate*, *31*(2), 895–918.

Lu, J., Xue, D., Leung, L. R., Liu, F., Song, F., Harrop, B., & Zhou, W. (2021). The leading modes of Asian summer monsoon variability as pulses of atmospheric energy flow. *Geophysical Research Letters*, *48*. https://doi.org/10.1029/2020GL091629

Luo, Z. J., Anderson, R. C., Rossow, W. B., & Takahashi, H. (2017). Tropical cloud and precipitation regimes as seen from near-simultaneous TRMM, CloudSat, and CALIPSO observations and comparison with ISCCP. *Journal of Geophysical Research: Atmospheres*, *122*(11), 5988–6003. https://doi.org/10.1002/2017jd026569

Ma, H.-Y., Xie, S., Klein, S., Williams, K., Boyle, J., Bony, S., et al. (2014). On the correspondence between mean forecast errors and climate errors in CMIP5 models. *Journal of Climate*, *27*(4), 1781–1798. https://doi.org/10.1175/jcli-d-13-00474.1

Neelin, J. D. (2007). Moist dynamics of tropical convection zones in monsoons, teleconnections, and global warming. *The Global Circulation of the Atmosphere*, *267*, 301.

Peterson, H. G., & Boos, W. R. (2020). Feedbacks and eddy diffusivity in an energy balance model of tropical rainfall shifts. *npj Climate and Atmospheric Science*, *3*, 11. https://doi.org/10.1038/s41612-020-0114-4

Plumb, R. A. (2007). Dynamical constraints on monsoon circulations. *The Global Circulation of the Atmosphere*, *252*, 266.

Popp, M., & Silvers, L. G. (2017). Double and single ITCZS with and without clouds. *Journal of Climate*, *30*(22), 9147–9166. https://doi.org/10.1175/jcli-d-17-0062.1

Privé, N. C., & Plumb, R. A. (2007). Monsoon dynamics with interactive forcing. Part II: Impact of eddies and asymmetric geometries. *Journal of the Atmospheric Sciences*, *64*(5), 1431–1442. https://doi.org/10.1175/jas3917.1

Rajeevan, M., & Srinivasan, J. (2000). Net cloud radiative forcing at the top of the atmosphere in the Asian monsoon region. *Journal of Climate*, *13*(3), 650–657. https://doi.org/10.1175/1520-0442(2000)013<0650:ncrfat>2.0.co;2

Randall, D. A., Dazlich, D. A., & Corsetti, T. G. (1989). Interactions among radiation, convection, and large-scale dynamics in a general circulation model. *Journal of the Atmospheric Sciences*, *46*(13), 1943–1970. https://doi.org/10.1175/1520-0469(1989)046<1943:iarcal>2.0.co;2

Saha, S., Moorthi, S., Wu, X., Wang, J., Nadiga, S., Tripp, P., et al. (2014). The NCEP climate forecast system version 2. *Journal of Climate*, *27*(6), 2185–2208. https://doi.org/10.1175/jcli-d-12-00823.1

Saud, T., Dey, S., Das, S., & Dutta, S. (2016). A satellite-based 13 yr climatology of net cloud radiative forcing over the Indian monsoon region. *Atmospheric Research*, *182*, 76–86. https://doi.org/10.1016/J.ATMOSRES.2016.07.017

Sharma, O. P. (1998). Interannual variations of summer monsoons: Sensitivity to cloud radiative forcing. *Journal of Climate*, *11*. https://doi.org/10.1175/1520-0442-11.8.1883

Shekhar, R., & Boos, W. R. (2016). Improving energy-based estimates of monsoon location in the presence of proximal deserts. *Journal of Climate*, *29*(13), 4741–4761. https://doi.org/10.1175/jcli-d-15-0747.1

Sherwood, S. C., Ramanathan, V., Barnett, T. P., Tyree, M. K., & Roeckner, E. (1994). Response of an atmospheric general circulation model to radiative forcing of tropical clouds. *Journal of Geophysical Research: Atmospheres*, *99*(D10), 20829–20845.

Slingo, A., & Slingo, J. (1988). The response of a general circulation model to cloud longwave radiative forcing. I: Introduction and initial experiments. *Quarterly Journal of the Royal Meteorological Society*, *114*(482), 1027–1062. https://doi.org/10.1002/qj.49711448209

Sohn, B.-J., & Smith, E. A. (1992). Global energy transports and the influence of clouds on transport requirements—A satellite analysis. *Journal of Climate*, *5*(7), 717–734. https://doi.org/10.1175/1520-0442(1992)005<0717:getati>2.0.co;2

Sperber, K., Annamalai, H., Kang, I.-S., Kitoh, A., Moise, A., Turner, A., et al. (2013). The Asian summer monsoon: An intercomparison of CMIP5 vs. CMIP3 simulations of the late 20th century. *Climate Dynamics*, *41*(9), 2711–2744. https://doi.org/10.1007/s00382-012-1607-6

Stevens, B., Bony, S., & Webb, M. (2012). Clouds on-off klimate intercomparison experiment (cookie).

Su, H., & Neelin, J. D. (2002). Teleconnection mechanisms for tropical Pacific descent anomalies during El niño. *Journal of the Atmospheric Sciences*, *59*. https://doi.org/10.1175/1520-0469(2002)059<2694:tmftpd>2.0.co;2

Tian, B., & Ramanathan, V. (2002). Role of tropical clouds in surface and atmospheric energy budget. *Journal of Climate*, *15*(3), 296–305. https://doi.org/10.1175/1520-0442(2002)015<0296:rotcis>2.0.co;2

Voigt, A., & Albern, N. (2019). No cookie for climate change. *Geophysical Research Letters*, *46*(24), 14751–14761. https://doi.org/10.1029/2019gl084987

Voigt, A., Bony, S., Dufresne, J.-L., & Stevens, B. (2014). The radiative impact of clouds on the shift of the intertropical convergence zone. *Geophysical Research Letters*, *41*(12), 4308–4315. https://doi.org/10.1002/2014gl060354

Voigt, A., & Shaw, T. A. (2015). Circulation response to warming shaped by radiative changes of clouds and water vapor. *Nature Geoscience*, *8*(2), 102–106. https://doi.org/10.1038/ngeo2345

Xie, S., Ma, H.-Y., Boyle, J. S., Klein, S. A., & Zhang, Y. (2012). On the correspondence between short-and long-time-scale systematic errors in CAM4/CAM5 for the year of tropical convection. *Journal of Climate*, *25*(22), 7937–7955. https://doi.org/10.1175/jcli-d-12-00134.1

Xie, S.-P., Tanimoto, Y., Noguchi, H., & Matsuno, T. (1999). How and why climate variability differs between the tropical Atlantic and Pacific. *Geophysical Research Letters*, *26*(11), 1609–1612. https://doi.org/10.1029/1999gl900308

Yu, L., & Weller, R. A. (2007). Objectively analyzed air-sea heat fluxes for the global ice-free oceans (1981–2005). *Bulletin of the American Meteorological Society*, *88*(4), 527–540. https://doi.org/10.1175/bams-88-4-527

Yuan, J., & Houze, R. A. (2010). Global variability of mesoscale convective system anvil structure from a-train satellite data. *Journal of Climate*, *23*(21), 5864–5888. https://doi.org/10.1175/2010jcli3671.1

Zeng, N., & Neelin, J. D. (1999). A land-atmosphere interaction theory for the tropical deforestation problem. *Journal of Climate*, *12*, 857–872. https://doi.org/10.1175/1520-0442(1999)012<0857:alaitf>2.0.co;2